Energy and angular momentum control of the specific opacity functions in the Ba +HI→BaI+H reaction

Cite as: J. Chem. Phys. **104**, 7947 (1996); https://doi.org/10.1063/1.471511
Submitted: 06 December 1995 . Accepted: 13 February 1996 . Published Online: 31 August 1998

Konstantinos S. Kalogerakis, and Richard N. Zare

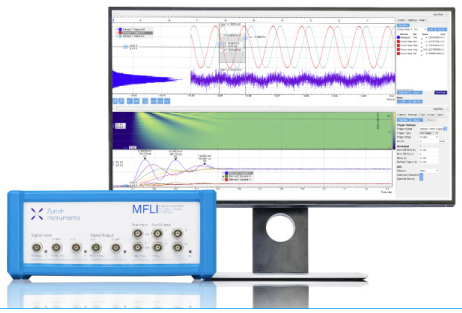

Energy and angular momentum control of the specific opacity functions in the Ba+HI→BaI+H reaction

Konstantinos S. Kalogerakis and Richard N. Zare
Department of Chemistry, Stanford University, Stanford, California 94305-5080

(Received 6 December 1995; accepted 13 February 1996)

Crossed-beam and beam-gas experiments on the reaction Ba+HI→BaI+H have been performed, in which the most probable collision energy ranges from 3 to 17 kcal/mol. The results, combined with previous experimental studies on this reaction system, show a remarkable collision energy dependence. Between low and high collision energies, a transition occurs in the intensity, width, and peak location of the product vibrational and rotational population distributions. The onset of this transition is estimated to occur at approximately 5 kcal/mol. For collision energies smaller than 5 kcal/mol, the product vibrational distribution is bell shaped and peaks at $v=12$. For collision energies larger than 5 kcal/mol, a second maximum appears at $v=0$ in the vibrational distribution. The rotational distributions of the crossed-beam experiments are extremely narrow but broaden at lower collision energies. As the collision energy is increased above 5 kcal/mol, the BaI rotational excitation is very near the energetic limit, and the maximum for the BaI($v=0$) rotational population distribution moves from $J=415.5$ to $J=538.5$. In contrast, below the transition onset, the maximum remains unchanged around $J=420.5$. Moreover, the peaks of the BaI($v=1$) and BaI($v=2$) rotational distributions appear at successively lower J values, as expected from energy conservation arguments. The nature of the kinematic constraints for this reaction allows the determination of the opacity functions for the production of the BaI product in a specific vibrational level v. Detailed analysis of the collision energy dependence of the specific opacity functions offers insight into the role of conservation of energy and angular momentum in influencing this reaction. At low collision energies, the maximum reactive impact parameter, $b_{\max}$, is determined by an angular momentum (centrifugal) barrier. At collision energies larger than 5 kcal/mol, conservation of energy dictates the value of $b_{\max}$. These two processes are identified as the mechanisms that control the Ba+HI reaction cross section. The transition between the two mechanisms provides an interpretation for the bimodal character of the BaI product internal-state distribution. © *1996 American Institute of Physics.* [S0021-9606(96)01419-7]

I. INTRODUCTION

The reactions of alkaline earth metal atoms with hydrogen halide molecules, M(Be, Mg, Ca, Sr, Ba)+HX(X=F, Cl, Br, I)→MX+H, have been studied extensively over the past 25 years.[1] The reactivity within this reaction family exhibits a particularly interesting behavior. Alkaline earth atoms have an ns^2 valence-shell electronic structure. Species of the type H–M–X, which result from insertion of the metal atom into the hydrogen halide bond, are stable and could be participating in a complex-mediated reaction mechanism. In other words, the divalent character of alkaline earth atoms manifests itself in the presence of a deep well in the potential energy surface of these reactions. Two possibilities appear for the transformation from reactants to products: a direct halogen abstraction pathway, which involves a harpoon mechanism, and an insertion pathway, in which the H–M–X potential well is sampled. In some reactions of this family, as in the Ca+HF reaction, the insertion pathway has been shown to be dominant,[2] whereas in others, such as the Ba +HBr and Ba+HCl reactions, the reactions appear to proceed through a direct abstraction pathway.[3,4]

The M+HX reaction family is also characterized by a special mass combination, namely, that of ''heavy atom +heavy-light diatomic molecule.'' The large difference between reactant and product reduced masses largely dictates the fate of the reactant angular momentum. The kinematic (mass) constraint results in efficient channeling of the reactant orbital angular momentum into product rotation.[5,6] As the mass of the metal and halogen atoms increases, the constraint on angular momentum conversion becomes more pronounced. The Ba+HI reaction system appears to be the most kinematically constrained system amenable to experimental study (without the handling of radioactive samples).

Competition between two distinctly different reaction pathways, if present, would lead to interesting dynamical behavior and could provide valuable information on the factors that affect the microscopic details of a chemical reaction. On the other hand, the requirements of the mass combination constrain the role of the potential energy surface. An interesting question arises: to what extent is the behavior of these systems dictated by the mass combination with respect to the features of the potential energy surface?

The kinematically constrained nature of this reaction system can be exploited to deduce its specific opacity functions, which are the impact parameter distributions that give rise to product in a specific vibrational level.[5,7] Consequently, a very detailed picture of the impact parameter dependence of this reaction can be acquired. The reagent im-

pact parameter of a bimolecular reaction cannot be experimentally controlled, except in a few isolated cases that involve photoinitiated reactions in van der Waals complexes.[8] Better understanding of the behavior of the specific opacity functions sheds light on the microscopic details of the relation between the reagent approach geometry, the transition-state region, and the reaction products.

The experimental results for this reaction system demonstrate a bimodal character, which will be presented in detail. Based on the well-established chemical reactivity trends and patterns within this reaction family, we previously suggested the possibility of a competition between two reaction mechanisms, namely, an abstraction and an insertion pathway.[1] In the present paper, the determination of the collision energy dependence of the reaction is used to demonstrate that the two reaction modes we observe correspond to two mechanisms that control the specific opacity functions. The two mechanisms are identified as (1) an angular momentum barrier that must be surmounted at low collision energies and (2) conservation of energy, which, at high collision energies, cuts off the maximum range of reactive impact parameters that yield BaI product in a given vibrational level. The transition between these two mechanisms as the collision energy is varied provides an interpretation for the experimentally observed bimodality in the BaI product vibrational and rotational population distributions.

II. EXPERIMENTAL TECHNIQUES AND METHODOLOGY

The experimental apparatus is described in detail elsewhere.[9] It consists of a scattering chamber, a laser system, and a fluorescence detection assembly. The reactants are generated in differentially pumped compartments of the scattering chamber. A laser beam probes the nascent BaI product in the reaction region, and the emitted fluorescence is collected and recorded by the detection system.

The reactant HI is prepared in its ground state either as a beam or as residual gas in the chamber. For the crossed-beam experiments, a seeded supersonic beam is generated by expansion through a 100 μm nozzle with backing pressures of approximately 200 kPa. Different carrier gases and seeding conditions are used to vary the attained kinetic energy. The beam is skimmed and collimated, and it enters the scattering region after propagation through two differentially pumped compartments. An appropriately positioned mechanical chopper in the second chamber can be rotated so as to intersect the beam. The HI beam velocity distribution can then be characterized by time-of-flight measurements using a mass spectrometer. In the beam-gas experiments, the HI gas is allowed to leak into the main chamber through a micrometer needle valve. Typical pressures in the scattering region are 7×10^{-4} Torr for beam-gas and 6×10^{-7} Torr for crossed-beam experiments. Under these conditions, the nascent product is probed before it undergoes any appreciable secondary collisions. The carrier and the HI gases are mixed and thoroughly stirred in a specially designed gas-handling manifold. In all experiments, the HI gas is purified from residual H_2 by freeze–pump–thaw degassing cycles using liquid N_2. Contamination by residual I_2 is minimized by keeping the HI lecture bottle at 0 °C while preparing the HI and carrier gas mixture.

A ground-state barium atom beam is generated by heating barium in a stainless steel crucible. The crucible has an orifice of 0.8 mm in diameter and is radiatively heated to approximately 1000 °C. The beam is collimated by a skimmer and a series of apertures. In the crossed-beam configuration, the barium beam and the supersonic HI beam intersect each other at right angles.

The laser system consists of a single-mode continuous-wave (cw) ring dye laser (Coherent 699-29) optically pumped by an argon ion laser (Spectra Physics 171-09). Rhodamine 560 perchlorate dissolved in ethylene glycol is the dye solution of choice. The output laser beam is spatially filtered and expanded to approximately 0.8 cm in diameter using a Keplerian telescope, and its intensity is actively stabilized. The beam is introduced into the scattering chamber at a right angle with respect to the plane of the Ba and HI beam axes. The reaction product is probed by detecting the laser-induced fluorescence (LIF) of the BaI $C-X$ transition. The narrow bandwidth of the laser makes possible high-resolution spectroscopic studies of the heavy BaI reaction product. The excitation power varies between 2 and 35 mW/cm^2, depending upon the type of measurement. In each case, the power is set to be as low as possible to minimize saturation of the transition.

The laser source is also being used to characterize the Ba beam velocity distribution by Doppler spectroscopy of the two-photon atomic transition $^3D_2-{}^1S_0$ at 36 200.42 cm^{-1}. In this case, the maximum attainable excitation power is used, and the beam is tightly focused. A sub-Doppler and a Doppler-limited spectrum are recorded with the laser beam at a 90° and at 45° with respect to the barium beam, respectively. From these data, the velocity distribution can be determined by employing a least-squares convolution-fit procedure.

Light from the reaction region is collected by a set of three lenses that minimize aberration. It is detected either directly by a photomultiplier tube or after being dispersed by a 1 m monochromator. The almost identical vibrational constants for the BaI C and X states and the very small rotational constant of BaI produce extremely congested spectra. A scheme of selectively detected LIF (SDLIF) is employed to simplify the spectra.[10] The emitted light is detected with a photon-counting system for SDLIF and with a lock-in amplifier when collected as total fluorescence. The SDLIF scheme follows the approach of previous work in our laboratory.[11,12] For each vibrational band under study, the R_{21} branch is excited and the emitted fluorescence is collected from the P_{21} and Q_2 branches. The monochromator transmission window for crossed-beam experiments differs from that of beam-gas experiments; it typically has a FWHM of 7 cm^{-1} for the former and 30 to 60 cm^{-1} for the latter. The adjustment of the transmission width for each experiment is the result of a compromise between loss of signal and loss of spectral resolution. Figure 1 demonstrates implementation of

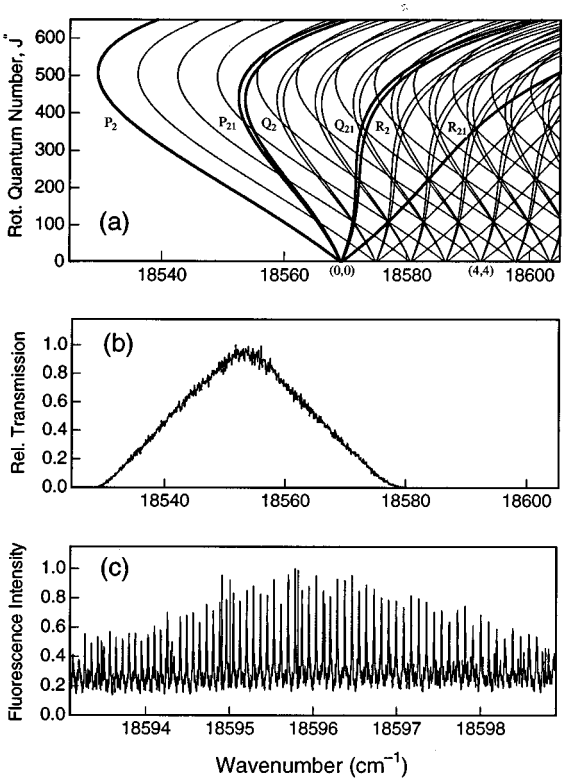

FIG. 1. The fluorescence selective detection scheme employed in the crossed-beam experiments. Panel (a) presents a Fortrat diagram for the BaI $C\ ^2\Pi_{3/2}-X\ ^2\Sigma^+$ $\Delta v=0$ sequence. The branches of the (0,0) member of the sequence are labeled on the corresponding curves. The origins of selected members of the $\Delta v=0$ sequence are also indicated below the abscissa. In panel (b), a typical transmission spectrum of the monochromator is shown. In this example, the location of the transmission window is selected in such a way that the monochromator transmission is maximum for emission near the bandheads of the P_{21} and Q_2 branches of the (0,0) band. The laser is scanned in a region of frequencies outside the monochromator transmission window, in which transitions of the R_{21} branch of the (0,0) band are excited. Fluorescence from such transitions can be emitted either in resonance or via the P_{21}- and Q_2-branch members of the (0,0) band, which share a common upper state with the R_{21} (0,0) transition. Therefore, a fraction of the emitted fluorescence is selectively transmitted through the monochromator and detected by the photomultiplier tube. Panel (c) displays an example of an excitation spectrum recorded with the presented monochromator transmission.

the SDLIF scheme for a crossed-beam experiment. Panel (a) presents a section of the Fortrat diagram for the $\Delta v=0$ sequence of the BaI $C\ ^2\Pi_{3/2}-X\ ^2\Sigma^+$ band, in which the branches of the (0,0) transition are labeled. Panel (b) shows the monochromator transmission spectrum and panel (c) the recorded excitation spectrum for this configuration. Without dispersion of the fluorescence, the overlaps are so extensive that an excitation spectrum in the same region would be impossible to analyze. The transmission spectrum of the monochromator is recorded for each experiment. In all measurements involving BaI or Ba, excitation spectra are recorded of the studied transitions. The laser power is monitored continuously, and iodine absorption spectra are obtained concurrently as a frequency reference.

The recorded BaI spectra can be analyzed to yield product rotational distributions. The spectroscopy of the BaI $C-X$ transition has been well established by extensive studies in our laboratory.[13–17] The rotational spectra are converted into relative population distributions by taking into account the excitation and emission probabilities and the monochromator transmission spectrum.

Crossed-beam experiments are conducted with collision energies between 5 and 17 kcal/mol. A beam-gas configuration is used to study the reaction product at collision energies less than 5 kcal/mol. The variation of experimental conditions within this range is sufficiently large to ensure a more comprehensive observation of the reaction system. Total undispersed fluorescence measurements provide low-resolution spectra that contain information on the product vibrational distributions. The SDLIF scheme is employed in the collection of spectra with rotational resolution from the three lowest vibrational levels $v=0$, 1, and 2.

The crossed-beam experiments extend the previous study of Vaccaro *et al.*,[18] who measured product rotational distributions and determined specific opacity functions for BaI($v=0$) in the range of 5 to 8 kcal/mol. Their experiments were performed in a crossed-beam configuration that detected total fluorescence from the BaI product. The nonselective total fluorescence detection scheme restricts the range of experimental conditions. Only the narrow, isolated region to the low-frequency side of the Fortrat diagram of Fig. 1 could provide useful spectra resulting from emission via the P_2-branch members of the (0,0), (1,1), and (2,2) bands. At collision energies higher than 8 kcal/mol, the reaction populates product BaI($v=0$) rotational states that lead to formation of a bandhead. Thus, the recorded total fluorescence spectra cannot be used for the determination of rotational population distributions. At collision energies lower than 5.5 kcal/mol, the product rotational distributions are significantly colder, so that the P_2 branches could be populated in the region where extensive overlaps occur with branches from neighboring vibrational levels. As was shown in Fig. 1, SDLIF removes many of the problems that arise from the complexity of the spectroscopic transitions in this system. For a long time, however, the use of a monochromator to disperse the emitted fluorescence has been a luxury afforded only by the strong signal of beam-gas experiments. Optimization of the experimental conditions has led to crossed-beam experiments with a selective fluorescence detection scheme. This capability has enabled us to perform measurements and determine product rotational distributions and specific opacity functions over a wide range of collision energies.

Figure 2 presents reagent velocity distributions in the laboratory frame and relative velocity distributions in the center-of-mass frame for three different experimental conditions. Panels (a) and (b) correspond to crossed-beam experimental conditions, whereas panel (c) presents a comparison with the relative velocity attained in a typical beam-gas experiment. The width of the relative velocity distribution is, as expected, larger in the beam-gas configuration. Under crossed-beam conditions, the relative velocity width is reduced with collision energy. This behavior is a result of the large difference in width between the barium atom beam and

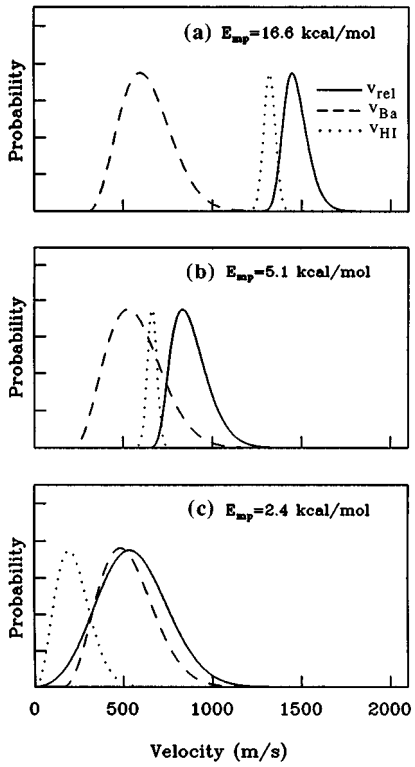

FIG. 2. Reagent velocity distributions in the laboratory frame and relative velocity distributions in the center-of-mass frame for experiments at different collision energies. Panels (a) and (b) correspond to crossed-beam conditions, whereas panel (c) represents a typical beam-gas experiment.

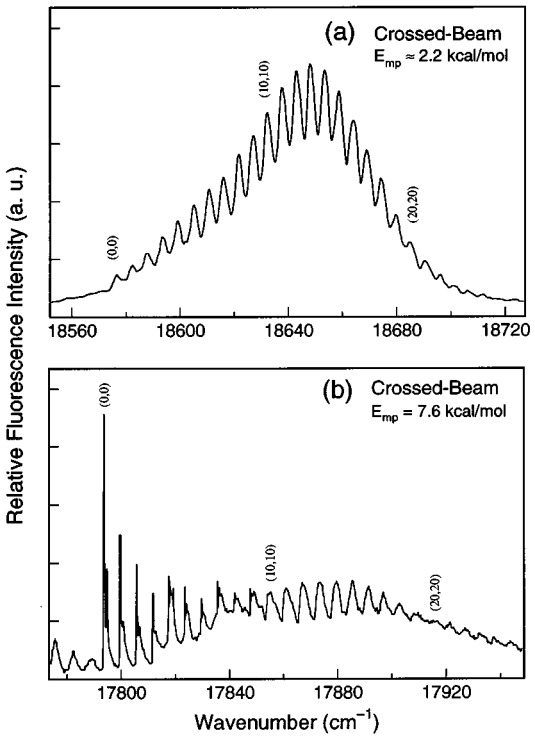

FIG. 3. Smoothed spectra covering the BaI $C\ ^2\Pi_{1/2}-X\ ^2\Sigma^+$ BaI $C\ ^2\Pi_{3/2}-X\ ^2\Sigma^+$ $\Delta v=0$ sequences. The spectra are recorded under crossed-beam conditions at two different collision energies. The laser is scanned over a wide frequency range with low resolution, and the LIF is detected by a photomultiplier tube without being dispersed by the monochromator. The $\Delta v=0$ sequence assignments that are mainly contributing to selected features in the spectrum are indicated. The upper spectrum is reproduced from Ref. 4 and the lower from Ref. 18.

the supersonic hydrogen iodide beam. When a light carrier gas is used for the supersonic HI beam, the HI velocity is much higher than the Ba velocities in the barium beam, and the relative velocity distribution resembles more closely that of the HI beam. In contrast, in a beam-gas or in a less energetic crossed-beam experiment, the velocities of the two reagents are of similar magnitude and, consequently, the features of the broader barium velocity distribution dominate. Figure 2 demonstrates that a broad range of reagent relative velocities is experimentally accessible. In addition, under different experimental conditions the reaction can be studied with distinctly different reagent relative velocity distributions.

III. VARIATION OF VIBRATIONAL AND ROTATIONAL DISTRIBUTIONS WITH COLLISION ENERGY

The product vibrational distribution shows unexpectedly different behavior between experiments conducted at high and low collision energies. Two results from previous studies in our laboratory are presented in Fig. 3. They are low-resolution excitation spectra covering the $\Delta v=0$ sequence of the BaI $C\ ^2\Pi_{1/2}-X\ ^2\Sigma^+$ and BaI $C\ ^2\Pi_{3/2}-X\ ^2\Sigma^+$ bands in a crossed-beam configuration. In both spectra, the LIF signal was collected nonselectively as total fluorescence. Extensive overlap exists between the different branches of neighboring members in the $\Delta v=0$ sequence. Nevertheless, because the $C-X$ transition is diagonal, the spectra provide a measure of the BaI product vibrational distribution and its collision energy dependence.

Figure 3(a) shows the result of the crossed-beam study employing LIF techniques of Cruse, Dagdigian, and Zare in 1973.[4] The BaI(v) distribution is bell shaped, and the maximum of the distribution is located at $v=12$. The same bell-shaped distribution has emerged from numerous beam-gas experiments in which an analysis is made of both BaI $C-X$ spin–orbit subbands.[19–23]

Figure 3(b) shows a contrasting result from the more energetic crossed-beam experiments of Vaccaro *et al.*,[18] who performed measurements with similar results in both spin–orbit subbands. In this spectrum, the dominant feature is found in the lowest vibrational levels. Moreover, the high rotational excitation of BaI for these lowest vibrational levels manifests itself in the pronounced appearance of the P_1Q_{12} and Q_1R_{12} bandheads. Vaccaro *et al.* extracted product rotational distributions for BaI($v=0$) from the low wave-number region to the left of the (0,0) P_1 bandhead. This region corresponds to the isolated P_{12}-branch members of the (0,0), (1,1), and (2,2) bands. Because no overlaps exist between the neighboring P_{12} branches of this region, the trend in the relative vibrational population can be established with confidence. Cruse *et al.*[4] estimated the most probable velocity in

TABLE I. The most probable relative velocity, v_{mp} (m/s), the most probable center-of-mass collision energy, E_{mp} (kcal/mol), and the FWHM, E_{FWHM} (kcal/mol), values corresponding to the energy distributions for the experiments presented in Sec. III. The experimental configuration is indicated in the first column.

Experiment	E_{mp} (kcal/mol)	v_{mp} (m/s)	E_{FWHM} (kcal/mol)
beam-gas	2.4	555	4.5
beam-gas	3.8	691	4.7
crossed-beam	5.1	805	3.6
crossed-beam	6.1	876	3.3
crossed-beam	7.0	937	3.2
crossed-beam	7.8	995	3.2

their experiment to be in the region of 2.2 kcal/mol, whereas the experiment shown in Fig. 3(b) had a most probable collision energy of 7.6 kcal/mol. Thus, at the higher energies, a significant portion of the reaction product appears in the lowest vibrational levels with the relative population order $v=0>v=1>v=2$. This trend is exactly the reverse of that encountered in the bell-shaped distribution of the experiments at lower collision energies [Fig. 3(a)].

Extensive efforts were made to observe the transition in the behavior of the reaction by systematically varying the collision energy. In the crossed-beam configuration, the lowest collision energy that could be achieved in our apparatus is approximately 5 kcal/mol, at which energy the behavior is similar to that described previously for the crossed-beam conditions. An alternative possibility was to vary the collision energy of the beam-gas experiments. The broad width of the barium velocity distribution and the relatively narrow range for oven temperature variations, however, limit the resolution of this approach. The temperature of the barium oven could range from 850 °C to 1200 °C. Thus, we could achieve a most probable collision energy as high as 3.8 kcal/mol with a 4.5 kcal/mol width (FWHM). Experiments at low oven temperature had a most probable collision energy of 2.4 kcal/mol and a width comparable to that at the higher temperatures. The latter experimental conditions compare closely with those of previous beam-gas studies.[11] Table I contains information on the reagent velocity distributions of the experiments presented in this section.

The difference in the relative velocity distributions between the low and high oven temperature experiments, which is shown in Fig. 4, is rather small. Nevertheless, the change between the beam-gas spectra of Fig. 5 at low and at high oven temperatures is dramatic. Quite remarkably, the small increase in collision energy causes the observed transition in the behavior of the reaction. This behavior is consistent with the crossed-beam results of Fig. 3. The shaded narrow band of the faster velocity distribution of Fig. 4 gives rise to the pronounced features in the low vibrational level portion of the spectrum in Fig. 5(b). Henceforth, we refer to the beam-gas experiments with low and high barium oven temperatures as ''slow'' and ''fast,'' respectively.

As a next step, rotationally resolved measurements were performed to observe the behavior of the lower vibrational levels in more detail. Figures 6(a) and 7(a) show the results

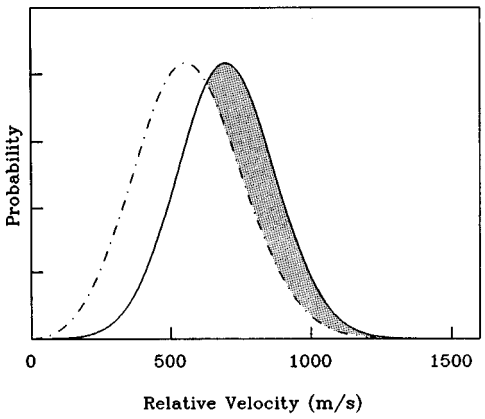

FIG. 4. Reagent relative velocity distributions for beam-gas conditions at low (dashed line) and high (solid line) barium oven temperatures. The shaded area corresponds to the increase in relative velocity caused by changing the oven temperature. This difference in the relative velocity causes the change in the spectra shown in Fig. 5.

for a slow and a fast beam-gas experiment with most probable collision energies of 2.4 and 3.8 kcal/mol, respectively. Overall, both distributions appear rather similar. The wide BaI($v=0$) product rotational distributions have maxima around rotational quantum number $J=425.5$ and a long tail that extends toward lower quantum numbers. The signal-to-noise ratio is better for the fast experiment, for which the maximum is clearly defined. Despite the presence of some

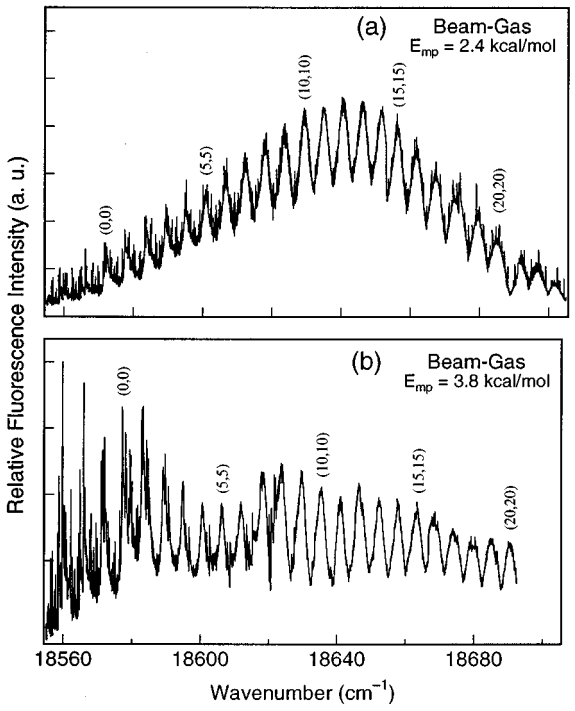

FIG. 5. Smoothed spectra covering the BaI $C\ ^2\Pi_{3/2}-X\ ^2\Sigma^+$ $\Delta v=0$ sequence from reaction under beam-gas conditions. The LIF is collected undispersed. The spectrum in panel (a) is taken from Ref. 11. The only difference between the two experiments is the barium oven temperature, which is higher by approximately 300 °C in the experiment shown in panel (b).

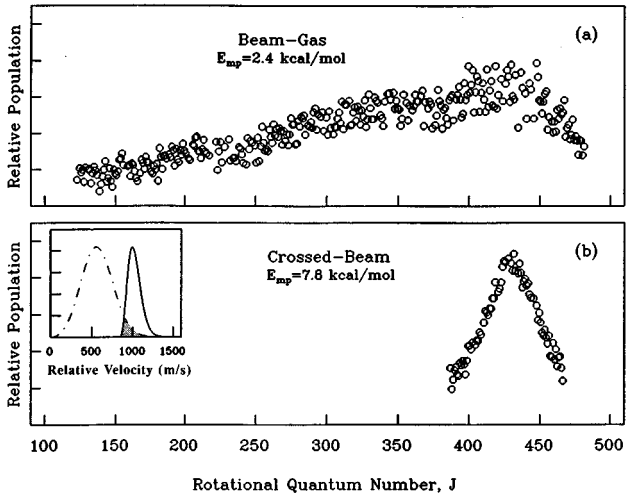

FIG. 6. BaI($v=0$) rotational distributions: (a) from a beam-gas experiment with E_{mp}=2.4 kcal/mol; and (b) from a crossed-beam experiment with E_{mp}=7.8 kcal/mol. The insert presents the reagent relative velocities for the two experiments. The overlap region of the two velocity distributions is shaded.

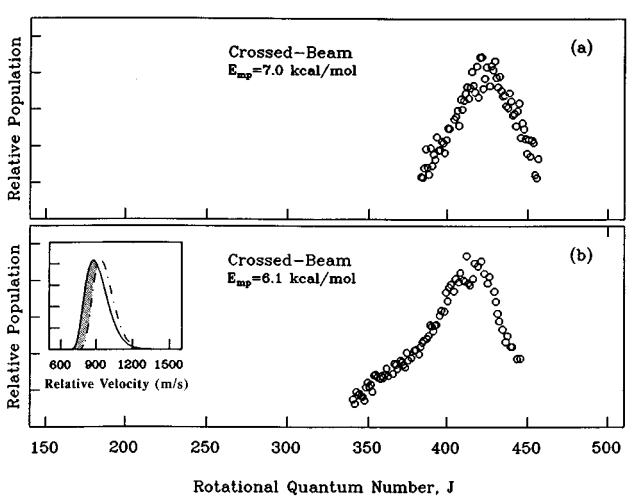

FIG. 8. BaI($v=0$) rotational distributions from crossed-beam experiments with (a) E_{mp}=7.0 kcal/mol and (b) E_{mp}=6.1 kcal/mol. The insert presents the reagent relative velocities for the two experiments. The shaded region is the low velocity band that is not common in the two distributions and is responsible for the observed difference in the corresponding product rotational distributions.

noise in the measurements, careful observation of Fig. 7(a) reveals a telltale sign of bimodality. Product rotational distributions recorded for vibrational levels $v=1$ and $v=2$ also suggest a bimodal character.

The rotational distributions for BaI($v=0$) in a beam-gas configuration reveal a remarkable behavior, as shown in Fig. 6, which presents a comparison between a beam-gas and a crossed-beam BaI($v=0$) rotational distribution, both recorded using SDLIF. Even though the overlap of the two relative velocity distributions is limited, both product distributions peak at similar J values. The peak in the BaI($v=0$) distribution from beam-gas experiments does not result from the most probable reagent relative velocity. Conservation of energy requires that the high-J portion of the distributions be produced from the high-energy fraction of the collision energy distribution. Tsekouras *et al.*[11] also made this observation in comparing their slow beam-gas experiments with the BaI($v=0$) crossed-beam study of Vaccaro *et al.*[18] Two distinct processes must be present that contribute to the observed results, as foreshadowed by the bimodality in the spectra of Figs. 3(b) and 5(b) and the shape of the beam-gas spectrum of Fig. 7(a). A comparison of the two distributions shown in Figs. 6(a) and 6(b) indicates that the process which yields BaI product with high rotational excitation is characterized by an energy threshold. The magnitude of this threshold coincides with the collision energies for which a transition was observed in the behavior of the vibrational distributions.

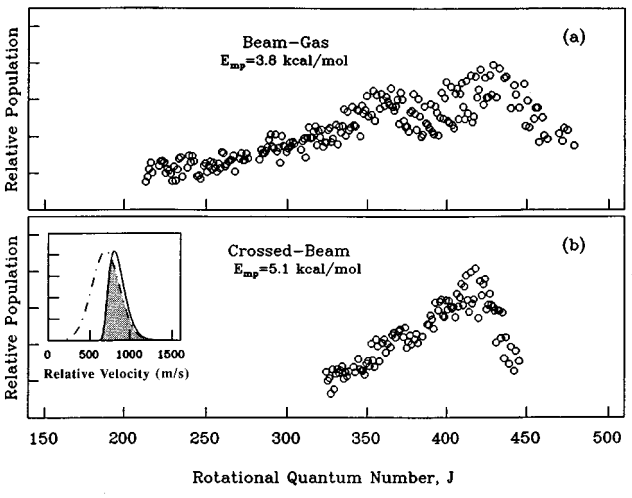

FIG. 7. BaI($v=0$) rotational distributions: (a) from a beam-gas experiment with E_{mp}=3.8 kcal/mol; and (b) from a crossed-beam experiment with E_{mp}=5.1 kcal/mol. The insert presents the reagent relative velocities for the two experiments. The overlap region of the two velocity distributions is shaded.

Another comparison that attempts to deepen the understanding of the transition region is that shown in Fig. 8, which presents BaI($v=0$) rotational distributions from crossed-beam experiments at most probable collision energies of 7.0 and 6.1 kcal/mol. Both distributions are very narrow, in agreement with previous observations.[18] The shoulder that appears to the low-J side of the distribution in panel (b) results from a narrow range of relative velocities, as shown in the insert. This shoulder grows gradually as the collision energy of the crossed-beam experiments is decreased below 6.5 kcal/mol, and, in the collision energy range of the beam-gas experiments, it represents a significant portion of the rotational distribution, as demonstrated in Fig. 6(a). This shoulder appears to be the signature of the second process, a process that becomes important at low collision energies.

The comparisons presented thus far show that the Ba+HI reaction exhibits a bimodal character as the collision energy is varied. The appearance of a new maximum at $v=0$

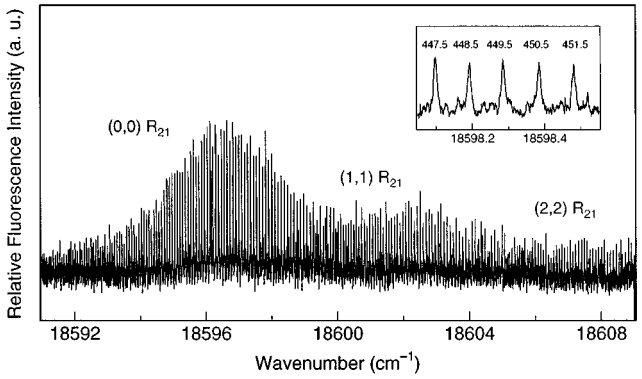

FIG. 9. Excitation spectrum of the BaI $C\ ^2\Pi_{3/2}-X\ ^2\Sigma^+$ R_{21}-branch members of the (0,0), (1,1), and (2,2) bands from reaction in an experiment conducted under crossed-beam conditions and with $E_{mp}=7.8$ kcal/mol. The LIF is selectively detected. The insert displays selected individual rotational lines in more detail.

in the vibrational population distribution of BaI and the changes in width and peak location of the rotational population distributions are all manifestations of a transition in reaction mode that occurs between low and high collision energies. From the experimental results, the energy threshold for the transition behavior is estimated to be in the region of 5 kcal/mol. In addition, the fact that the peak of the beam-gas BaI($v=0$) rotational distribution remains at high-J values, even when the most probable collision energy is well below the energetic requirements, reveals a difference in the relative probability of the two processes; the probability of producing BaI($v=0$), once above the energetic threshold, appears significantly higher than that at lower collision energies.

IV. BaI(v=0,1,2) ROTATIONAL DISTRIBUTIONS FROM CROSSED-BEAM EXPERIMENTS

Figure 9 shows a representative SDLIF spectrum from a crossed-beam experiment with a most probable collision energy of 7.8 kcal/mol. Three discrete distributions can be distinguished that correspond to emission from the BaI $v=0$, 1, and 2 vibrational levels. The spectrum also clearly shows that in this region of collision energies, the relative order of the rotational populations is $v=0>v=1>v=2$. The same relative order is found in all crossed-beam experiments.

Figure 10 presents product rotational distributions for BaI($v=0$). The simulated rotational distributions presented in the same figure will be discussed in Sec. V. In all experiments, the product rotational distributions are extremely narrow and peak at very large J. At low collision energies, a shoulder appears to the low-J side of the rotational distributions and grows as the collision energy is decreased further. This shoulder continues to grow even more at the lower collision energies of the beam-gas experiments.[11] We also observe a trend in the behavior of the peak locations of the rotational population distributions; the peaks appear at gradually larger J values as the collision energy is increased. Figure 11 displays the most probable rotational energy of

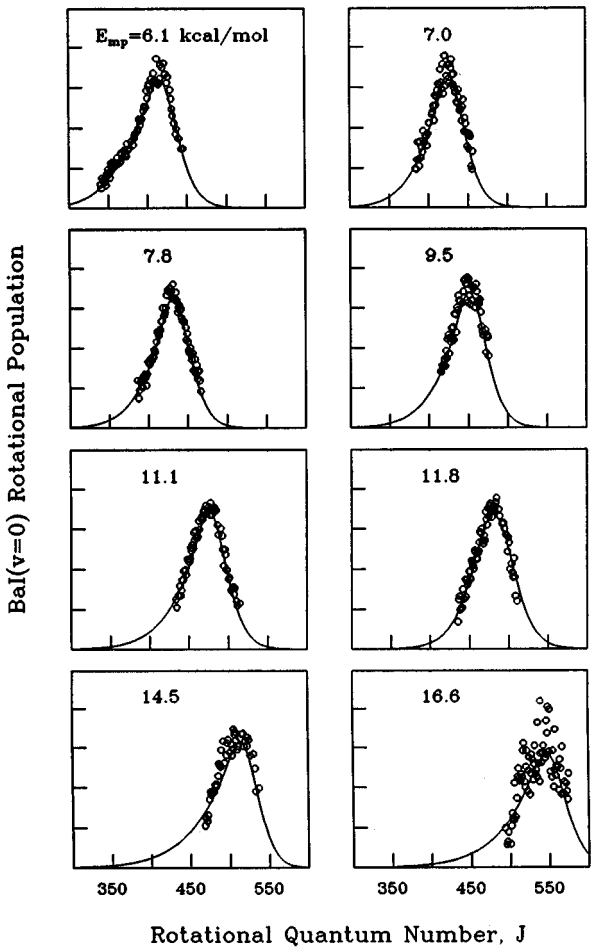

FIG. 10. BaI($v=0$) experimental and simulated rotational distributions from crossed-beam experiments at different collision energies.

BaI($v=0$), E_{rot}, as a function of the most probable collision energy, E_{mp}. The trend in the peak location of the distributions is very clear in this figure, as is the fact that most of the excess collision energy is channeled into product rotational energy.

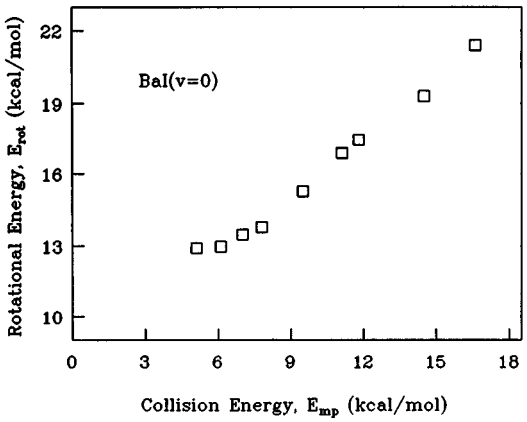

FIG. 11. The most probable BaI($v=0$) rotational energy, E_{rot}, as a function of the most probable collision energy, E_{mp}, for crossed-beam experiments.

TABLE II. Information on product BaI($v=0$) rotational distributions from crossed-beam experiments, in which the collision energy distribution has the most probable value, E_{mp}, and a width that is represented by the FWHM value. The BaI($v=0$) rotational distribution is characterized by its peak, J_{mp}, and its FWHM. The product vibrational (E_{vib}), rotational (E_{rot}), and recoil (E_{rec}) energies that correspond to the peak of the rotational distribution are also shown. Implicit is the assumption that the maximum of the collision energy distribution gives rise to the maximum of the product rotational distribution.

Collision energy		BaI($v=0$, J) distribution		Energy partitioning		
E_{mp} (kcal/mol)	FWHM (kcal/mol)	J_{mp} ($\hbar$)	FWHM (kcal/mol)	E_{vib} (kcal/mol)	E_{rot} (mp) (kcal/mol)	E_{rec} (mp)[a] (kcal/mol)
6.1	3.3	416.5	3.4	0.2173	12.99	0.19
7.0	3.2	424.5	3.1	0.2173	13.49	0.59
7.8	3.2	429.5	3.2	0.2173	13.80	1.1
9.5	3.2	452.5	3.2	0.2173	15.28	1.3
11.1	3.4	476.5	4.0	0.2173	16.89	1.3
11.8	4.3	484.5	4.2	0.2173	17.45	1.4
14.5	3.1	510.5	4.1	0.2173	19.31	2.3
16.6	3.9	538.5	5.1	0.2173	21.40	2.3

[a]Assuming D_0^o(BaI)=77.7 kcal/mol.

Table II presents the widths and most probable values of the rotational and collision energy distributions in each experiment, as well as information on the partitioning of the available energy for the BaI($v=0$) reaction product. The widths of the collision energy and the product rotational energy distributions are very similar, foreshadowing that narrow specific opacity functions should be expected. In addition, this observation justifies the treatment, presented in Table II, that extracts information on the partitioning of product energy by assuming a one-to-one correspondence between the most probable values of the reagent collision and product rotational distributions. Inspection of the last column of Table II indicates a trend in the product recoil energy, which increases with increasing collision energy. In all experiments, the rotational excitation observed for BaI($v=0$) is very near the energetic limit; almost all the available energy for reaction appears as rotational excitation. This last observation will prove useful in our presentation later in this paper of the assumptions used for the determination of the specific opacity functions and in our discussion of the mechanisms that determine the reaction cross section.

Figure 12 shows results for BaI($v=1$) and BaI($v=2$), in which the observed trends are similar to those presented previously for BaI($v=0$). The signal for $v=1$ and $v=2$ is substantially lower. Only the unambiguous stronger lines near the peak of the distributions were considered for the extraction of the product rotational distribution points. As shown in Table III, the peaks of the rotational distributions appear at lower rotational quantum numbers as the vibrational energy is increased. This result is in agreement with conservation of energy arguments, provided that the product recoil does not decrease with vibrational excitation. Tables IV and V provide similar information for BaI($v=1,2$) as did Table II for BaI($v=0$). The two tables indicate that for BaI($v=1,2$), most of the available energy is channeled into rotation. Moreover, the product recoil energy appears to increase with increasing vibrational excitation. Therefore, the decrease in rotational excitation for higher vibrational levels of BaI is larger than that expected if the recoil energy were to remain constant, independent of the BaI(v,J) level produced by the reaction.

V. BaI($v=0,1,2$) SPECIFIC OPACITY FUNCTIONS

The kinematic constraints of the Ba+HI reaction provide a special opportunity to elucidate the influence of the approach geometry on the outcome of the reaction. The large

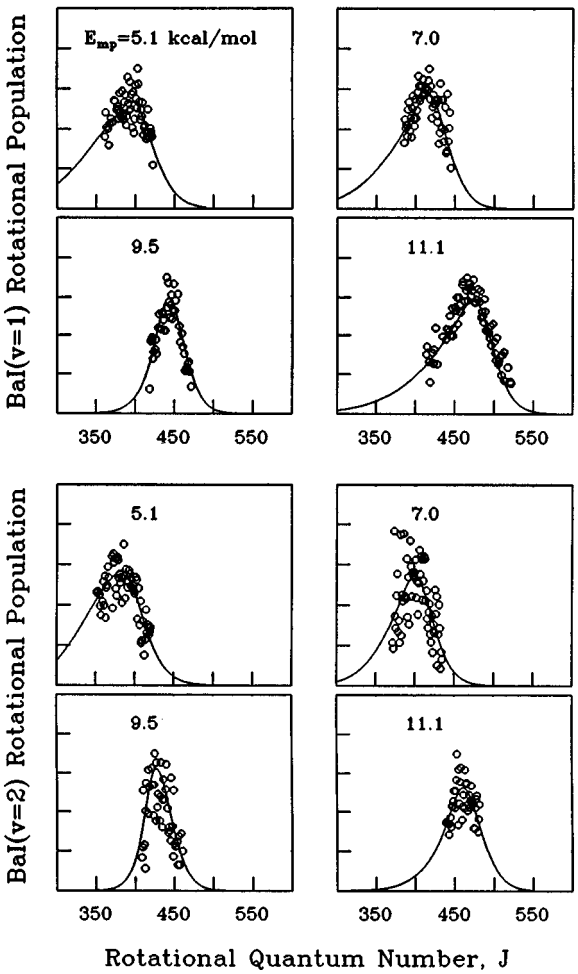

FIG. 12. Experimental and simulated rotational distributions for product BaI($v=1$) and BaI($v=2$) from crossed-beam experiments at different collision energies.

TABLE III. The most probable rotational quantum numbers, J_{mp}, for product distributions in vibrational levels $v=0$, $v=1$, and $v=2$, for crossed-beam experiments conducted at different collision energies.

E_{mp} (kcal/mol)	BaI($v=0$) J_{mp} ($\hbar$)	BaI($v=1$) J_{mp} ($\hbar$)	BaI($v=2$) J_{mp} ($\hbar$)
5.1	415.5	384.5	378.5
5.5	418.5	393.5	384.5
7.0	424.5	412.5	404.5
9.5	452.5	443.5	422.5
11.1	476.5	468.5	452.5

difference between reagent and product reduced masses results in almost exclusive channeling of the reagent orbital angular momentum $\mathbf{L}_{reag}$ into product rotational angular momentum $\mathbf{J}_{prod}$. The magnitude of $\mathbf{L}_{reag}$ is given by the equation

$$|\mathbf{L}_{reag}| = \mu |\mathbf{v}_{rel}| b, \tag{1}$$

where μ is the reagent reduced mass, $|\mathbf{v}_{rel}|$ is the magnitude of the reagent relative velocity in the center-of-mass frame, and b is the impact parameter for the reactive encounter. Thus, for this reaction we can write the approximation

$$\mu |\mathbf{v}_{rel}| b \approx |\mathbf{J}_{BaI}|, \tag{2}$$

where $|\mathbf{J}_{BaI}|$ represents the magnitude of the product BaI rotational angular momentum vector. This second equation sets the stage for experiments that provide indirect information on the distribution of reactive impact parameters that cause the formation of the BaI product in a specific vibrational level. Experimental determination of the product rotational distribution in a specific vibrational level and characterization of the reagent relative velocity distribution provides sufficient information to deduce the specific opacity functions by means of Eq. (2). Variation of the reagent relative velocity over a wide range can reveal the effect of the collision energy on the specific opacity functions. In all cases, the determined specific opacity functions represent an average over the angle of relative reagent orientation. Evidence from quasiclassical trajectory calculations,[6] however, indicates that the effect of reagent orientation for this mass combination is not expected to be significant. The small moment of inertia of the hydrogen halide makes possible its fast reorientation during the reactive encounter.

TABLE IV. Information on product BaI($v=1$) rotational distributions from crossed-beam experiments, presented in a similar manner as in Table II.

Collision energy		BaI($v=1$, J)	Energy partitioning		
E_{mp} (kcal/mol)	FWHM (kcal/mol)	J_{mp} ($\hbar$)	E_{vib} (kcal/mol)	E_{rot} (mp) (kcal/mol)	E_{rec} (mp)[a] (kcal/mol)
5.1	3.6	384.5	0.6507	11.08	0.67
5.5	3.6	393.5	0.6507	11.60	0.55
7.0	3.2	412.5	0.6507	12.72	0.93
9.5	3.2	443.5	0.6507	14.69	1.5
11.1	3.4	468.5	0.6507	16.35	1.4

[a]Assuming D_0^o(BaI)=77.7 kcal/mol.

TABLE V. Information on product BaI($v=2$) rotational distributions from crossed-beam experiments, presented in a similar manner as in Table II.

Collision energy		BaI($v=2$, J)	Energy partitioning		
E_{mp} (kcal/mol)	FWHM (kcal/mol)	J_{mp} ($\hbar$)	E_{vib} (kcal/mol)	E_{rot} (mp) (kcal/mol)	E_{rec} (mp)[a] (kcal/mol)
5.1	3.6	378.5	1.083	10.72	0.60
5.5	3.6	384.5	1.083	11.05	0.67
7.0	3.2	404.5	1.083	12.21	1.0
9.5	3.2	422.5	1.083	13.29	2.4
11.1	3.4	452.5	1.083	15.20	2.1

[a]Assuming D_0^o(BaI)=77.7 kcal/mol.

Vaccaro *et al.*[18] have rigorously examined the validity of the approximations of Eq. (2) under the conditions of a crossed-beam experiment. They concluded that this reaction system provides a prototypical example of a kinematically constrained reaction system that is suitable for the experimental determination of specific opacity functions. More specifically, the electronic and the rotational angular momenta of the reagents are negligible, as is the electronic orbital angular momentum of the hydrogen atom. Finally, the orbital angular momentum that arises from the recoil of the products is very small compared with the BaI rotational angular momentum and thus can be ignored. Consequently, application of the law of angular momentum conservation leads to Eq. (2). The experimental conditions of our study are similar to those of Vaccaro *et al.*, so that all of the above approximations are equally justifiable.

Noda *et al.*[12] performed experiments on the specific opacity function for BaI($v=8$) in a beam-gas configuration. In this study, the specific opacity function was expanded in terms of Dirac delta functions and the expansion coefficients were determined using a least-squares fitting method. Their study examined the influence of various models accounting for the relative velocity dependence of the reaction probability. Analysis of the data did not necessitate the incorporation of any specific velocity dependence scheme, and they determined that only a relatively narrow range of impact parameters contributes to the formation of the BaI($v=8$) product.

Vaccaro *et al.*[18] studied the reaction product BaI($v=0$) in a crossed-beam apparatus. The narrow relative velocity distribution of their crossed-beam experiments provided information that was not averaged over a wide range of velocities. Comparison of their results with those of Noda *et al.*[12] showed that the width of the relative velocity distribution plays a substantial role in shaping the product rotational distributions; the velocity-independent scheme of Noda *et al.* for modeling the specific opacity functions predicted rotational distributions much broader than the distributions observed under crossed-beam conditions. Vaccaro *et al.* realized that modeling of the results for BaI($v=0$) requires a rigorous application of both angular momentum and energy conservation. As was also predicted by the studies of Siegel and Schultz,[6] the total cross section for kinematically constrained reactions decreases with increasing relative velocity. Energy conservation sets an upper bound on the product ro-

tational excitation for a given product vibrational level that depends on the relative velocity. For each value of the reagent relative velocity, a maximum value occurs for the reactive impact parameter, which is dictated by conservation of energy. Reaction at larger impact parameters would lead to product with more rotational energy than the total available energy for reaction and hence cannot occur.

Vaccaro *et al.*[18] determined the specific opacity function for BaI($v=0$), which is denoted by $P_0(b)$. The model specific opacity function was convoluted with the relative velocity distribution, $f(v_{\rm rel})$, and the simulated rotational distribution, $n_0(J)$, was optimized to fit the the experimentally observed one. The convolution integral that yields the rotational population distribution, $n_v(J)$, in vibrational level v can be written as

$$n_v(J)=C\int_0^\infty bP_v(b)f(v_{\rm rel})dv_{\rm rel}, \tag{3}$$

where C is a constant different for each experiment.[19–23] The constraint of angular momentum conservation, as expressed in Eq. (1), has been incorporated in the derivation of Eq. (3). A hard-sphere model representing the specific opacity function as a step function was found inadequate. Another model investigated by Vaccaro *et al.* was based on a theoretical study of Noda and Zare,[24] who proposed a constant product recoil energy for all collision energies and product vibrational levels. This model, which corresponds to a reactive impact parameter distribution that is a Dirac delta function, provided a much better description of the experimental results and indicated that a small finite width in the form of the specific opacity function would improve the quality of the fit. The best agreement between simulation and experiment was obtained with fixed and moving Gaussian functions that were truncated at the energetic limit of the reaction. In the ''fixed truncated Gaussian'' model, the specific opacity function $P_v(b,v_{\rm rel})$ is given by the equation

$$P_v(b)=\exp\left[-\frac{1}{2}\left(\frac{b-\beta_v}{\sigma_v}\right)^2\right]H[b_{\rm max}(v_{\rm rel})-b], \tag{4}$$

where β_v represents the peak location of the Gaussian and σ_v is proportional to its width. The quantity $H[b_{\rm max}(v_{\rm rel})-b]$ corresponds to the Heavyside function,

$$H[b_{\rm max}(v_{\rm rel})-b]=\begin{cases}1, & b\leqslant b_{\rm max}\\ 0, & b\geqslant b_{\rm max},\end{cases} \tag{5}$$

which incorporates the truncation of the gaussian function necessitated by energy conservation. For the convolution fit, the adjustable parameters are β_v, σ_v, and D_0^o(BaI), the dissociation energy of BaI, which is necessary for the application of energy conservation and the subsequent determination of the maximum allowed impact parameter. This model has also been used successfully by Tsekouras *et al.*[11] to determine specific opacity functions for BaI($v=0$–18) in a beam-gas configuration.

The present experimental results cover a range of collision energies that is significantly wider than that of previous studies. Consequently, we can investigate more extensively the relative velocity dependence of the specific opacity functions for different vibrational levels. The data analysis is based on the previous models. None of them, however, can provide reasonable simulations over the entire range of collision energies studied. The reason for this behavior can be attributed to a change of the product recoil energy as the reagent collision energy is varied. As mentioned previously, Tables II, IV, and V indicate a trend in which the product recoil energy increases with collision energy. Including such a degree of freedom provides a significant improvement in the simulations, as demonstrated in the following discussion. For the fits that will be presented, we employed a slightly modified version of the ''fixed truncated Gaussian'' model.[18] The functional form of the specific opacity function is identical to that presented in Eq. (4). The adjustable parameters are β_v and σ_v, which are identical to the previous treatment, and ΔE_v, which is the difference between D_0^o(BaI) and the product recoil energy, $E_{\rm rec}$, at the maximum reactive impact parameter. The value of $E_{\rm rec}$ represents the minimum recoil energy at a given relative velocity. Because the specific opacity functions are sharply peaked, a limited range of recoil energies greater than or equal to $E_{\rm rec}$ is allowed for each relative velocity. The value of $E_{\rm rec}$ is representative of this narrow range. The ΔE_v parameter is optimized for each experiment and not globally. Because the range of relative collision energies is narrow and well defined in each crossed-beam experiment, this approach is tantamount to treating the product recoil energy as an additional degree of freedom.

TABLE VI. Numerical values for the adjustable parameters that describe the BaI($v=0$) specific opacity functions, as determined from the convolution-fit procedure. The 1σ uncertainties for the last quoted digit of the optimized values are indicated in parentheses. The simulated product rotational distributions are shown in Fig. 10.

	BaI($v=0$)		
$E_{\rm mp}$ (kcal/mol)	β_0[a] (Å)	σ_0 (Å)	ΔE_0[b] (kcal/mol)
6.1	5.2	0.65 (2)	79.00 (3)
7.0	5.2	0.58 (2)	78.65 (3)
7.8	5.2	0.62 (2)	78.09 (2)
9.5	5.2	0.66 (2)	77.65 (4)
11.1	5.2	0.70 (2)	77.71 (3)
11.8	5.2	0.53 (2)	77.86 (4)
14.5	5.2	0.81 (4)	77.07 (8)
16.6	5.2	0.76 (6)	77.6 (2)

[a]Fixed.
[b]$\Delta E_0=D_0^o({\rm BaI})-E_{\rm rec}(v=0)$.

Figure 10 presents simulated product rotational distributions for BaI($v=0$). The agreement with the experimental distributions is very satisfactory. The fits reproduce consistently the behavior of the rotational population distributions over the range of collision energies studied. Table VI presents the numerical results for the fits of the BaI($v=0$) distributions. Allowing all adjustable parameters to vary in the fitting routine led to instabilities. Therefore, the location of the Gaussian was optimized independently for the different collision energies by fixing the width at various values. The optimized value for the location of the peak of the Gaussian

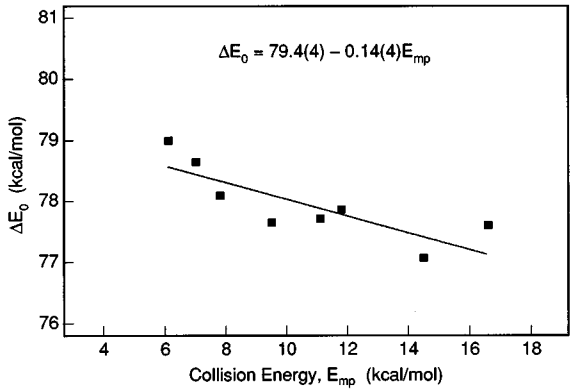

FIG. 13. The deduced ΔE_0 parameters plotted as a function of the most probable collision energy, E_{mp}. A linear fit is also shown along with the regression coefficients and their corresponding 1σ deviations in parentheses.

is 5.2 Å, and this value was kept fixed for all the simulations. This result agrees within error bars with the 5.14 (9) Å that Vaccaro *et al.*[18] found in their study. Similarly the optimized σ_v values are also in good agreement with the value of 0.59 (3) Å found by Vaccaro *et al.*[18] In other words, the specific opacity functions for BaI($v=0$) are extremely narrow over this broad energy range. This result is consistent with the observation of comparable widths for the rotational and collision energy distributions, and justifies the assumption used in Table II to extract information on the energy partitioning of the reaction. The only substantial difference between our results and those of Vaccaro *et al.* is in the parameter ΔE_v. Vaccaro *et al.*[18] used the value of D_0^o(BaI) as an adjustable parameter and assumed that the truncation of the Gaussian occurs at the energetic limit, in which all the available energy appears as product rotation. In contrast, this analysis incorporates a variable product recoil energy, which is the key feature leading to the presented fits. From Table VI we can observe a change of approximately 1.5 kcal/mol for the parameter ΔE_0 under the conditions studied. This change corresponds to a change in recoil energy and is consistent with the variation in the product recoil indicated in Table II. In addition, the value of ΔE_0=78.65 (3) kcal/mol, determined at a relative collision energy of 7.0 kcal/mol, is similar to the value of 78.48 (1) kcal/mol that Vacarro *et al.*[18] found for their corresponding adjustable parameter D_0^o(BaI).

Figure 13 displays the ΔE_0 values as a function of collision energy and a linear interpolation that succeeds in describing the variation of the product recoil with collision energy. The regression coefficients and their associated 1σ coefficients are shown in the figure. A clear trend is indicated, in which the product recoil energy increases with increasing collision energy. The possibility that the recoil energy should be expanded to higher order than zeroth was suggested by Noda and Zare,[24] but before this study no reason existed for this more complicated treatment. Consequently, the results of the present experiments provide the incentive to extend existing models put forth to describe the dynamics of kinematically constrained reactions, such as the constant product recoil model[24] and the constant product orbital angular momentum model.[25]

A similar treatment has been carried out for BaI($v=1$) and BaI($v=2$). The results are shown in Fig. 12. The fits are again very satisfactory. The adjustable parameters, which were optimized as in the case of $v=0$, are shown in Table VII. We note that the location of the peak in the specific opacity function moves successively to lower impact parameters by 0.3 Å as the vibrational level changes from $v=0$ to $v=1$ and $v=2$. The change of the parameters ΔE_1 and ΔE_2 as the collision energy is varied exhibits the same trend as in BaI($v=0$); their decrease with collision energy indicates an increase in the product recoil as the collision energy is increased. In addition, comparison of the results for $v=0$, 1, and 2 hints another trend: the product recoil appears to slowly increase with BaI vibrational excitation, by approximately 0.2 kcal/mol for $v=1$ and 0.7 kcal/mol for $v=2$. These differences happen to be similar to the vibrational energy differences between the corresponding levels.

VI. DISCUSSION

The reactions of alkaline earth metal atoms with hydrogen halides have been studied extensively over the past 25 years. A unifying theme for the reactivity within this reaction family has emerged from these studies: A competition exists between a direct harpoon mechanism, which involves abstraction of the halogen atom by the alkaline earth metal, and an insertion mechanism, in which the alkaline earth atom inserts in the hydrogen halide bond to form a short-lived intermediate.[1] The reaction exothermicity, the hydrogen halide vibrational excitation, and the reagent collision energy have been suggested as factors that influence the extent to which each reaction pathway is present.[1] A correlation appears to exist within this reaction family, in which the exothermic members tend to proceed through direct abstraction, whereas the endothermic ones exhibit a propensity for the insertion pathway. The presence of a substantial energetic barrier also appears to promote the formation of the intermediate complex. Direct halogen abstraction is dominant for Ba+HCl($\Delta H_0^o=-9.2$ kcal/mol) and Ba+HBr($\Delta H_0^o=-12.2$ kcal/mol).[3] Experimental and theoretical studies of the endothermic ($\Delta H_0^o=+14.8$ kcal/mol) Ca+HF reaction have revealed the importance of the long-lived H–Ca–F complex and indicated that the insertion pathway plays a dominant role for this reaction.[26–28] Based on theoretical calculations for the exothermic Be+HF reaction system[29–36] ($\Delta H_0^o=-6$ kcal/mol), which has a barrier height estimated at 19 kcal/mol,[36] a substantial number of reactive trajectories sample the deep potential well, thereby indicating the importance of the insertion mechanism. Other theoretical studies have extensively investigated this reaction mechanism duality for the endothermic reaction system Mg+HF[37–42] ($\Delta H_0^o=+30$ kcal/mol). In addition, the behavior of the less endothermic ($\Delta H_0^o=+6.4$ kcal/mol)Sr+HF reaction[27,28,43–46] was interpreted as a manifestation of the competition between insertion and direct abstraction.[28] Increase of the reagent vibrational excitation was suggested to favor the inser-

tion mechanism, whereas the reagent rotational excitation appeared to promote halogen abstraction.[27,28,45]

The Ba+HI reaction demonstrates a bimodal character in the internal-state population distributions, as presented in detail in Sec. III of the present paper. Based on available experience with the alkaline earth metal plus hydrogen halide reaction family, we previously attempted to interpret the observed bimodality as a competition between the insertion and abstraction pathways.[1] To verify this hypothesis, however, the following questions need to be addressed in some detail: What makes this exothermic reaction—otherwise so similar to Ba+HCl and Ba+HBr—behave in such a distinct way? Does the kinematically constrained nature of this reaction system play a substantial role in shaping, or even dictating, the features of the observed bimodality? In the present paper, detailed analysis of the specific opacity functions is employed as a tool to answer these questions. Our analysis indicates that the experimentally observed bimodality for the Ba+HI reaction system is not a manifestation of competition between an insertion and an abstraction mechanism. In contrast, it reveals the role of the centrifugal barrier and the conservation of energy in controlling the reaction cross section and determining the relative velocity dependence of the specific opacity functions for this kinematically constrained reaction system. The bimodal behavior is shown to arise from the transition between these two mechanisms that dictate the value of the maximum impact parameter: a centrifugal barrier at low collision energies and conservation of energy at high collision energies.

Because of the extremity of its mass combination, the Ba+HI reaction system does not lend itself favorably to theoretical calculations. Zhao and Zare[47] performed quasiclassical trajectory simulations for this system using a barrierless London–Eyring–Polanyi–Sato potential energy surface that favored a collinear approach. The results were in qualitative agreement with trends observed in the experiments, but they did not reveal any signs of bimodality. These simulations, however, were performed to provide a comparison with the crossed-beam work of Vaccaro *et al.*[18] and, consequently, no emphasis was placed on the low collision energy regime. A recent quasiclassical trajectory calculation study by Albertí *et al.*[48] investigated angular momentum vector correlations for this reaction system and focused its attention on the channeling of reagent rotational angular momentum into product orbital angular momentum. These results, however, cannot be directly compared with our experimental findings for $v=0,1,2$, which involve much larger impact parameters. Extension of the theoretical studies to simulate the currently available experimental results would further deepen the understanding of this reaction system.

In Sec. V, we presented a model for the specific opacity functions that succeeds in simulating the experimentally observed rotational distributions and accounting for the relative velocity dependence of the BaI($v=0,1,2$) specific opacity functions. This model employs a fixed Gaussian function that is subjected to the constraint of energy conservation and allows for a variable product recoil energy. As an example of the effect of the relative velocity on the specific opacity function, we note that the maximum allowed impact parameter for BaI($v=0$) moves from 4.6 Å for a relative velocity of 940 m/s to 3.7 Å for 1500 m/s.

TABLE VII. Numerical values for the adjustable parameters that describe the BaI($v=1$) and BaI($v=2$) specific opacity functions, as determined from the convolution-fit procedure. The 1σ uncertainties for the last quoted digit of the optimized values are indicated in parentheses. The simulated product rotational distributions are shown in Fig. 12.

	BaI($v=1$)			BaI($v=2$)		
E_{mp} (kcal/mol)	β_1[a] (Å)	σ_1 (Å)	ΔE_1[b] (kcal/mol)	β_2[a] (Å)	σ_2 (Å)	ΔE_2[c] (kcal/mol)
5.1	4.9	0.8 (2)	79.1 (1)	4.6	0.5 (2)	78.7 (1)
7.0	4.9	0.79 (1)	78.5 (1)	4.6	0.5 (1)	77.8 (1)
9.5	4.9	0.42 (4)	77.45 (6)	4.6	0.32 (5)	76.8 (1)
11.1	4.9	0.88 (5)	78.04 (7)	4.6	0.5 (1)	77.4 (1)

[a]Fixed.
[b]$\Delta E_1 = D_0^o(\mathrm{BaI}) - E_{rec}(v=1)$.
[c]$\Delta E_2 = D_0^o(\mathrm{BaI}) - E_{rec}(v=2)$.

The specific opacity functions are found to be centered around smaller impact parameters as the vibrational excitation is increased. Such behavior has been predicted for kinematically constrained systems and is consistent with an impulsive model, in which a negative correlation exists between the reactive impact parameter and the product vibrational excitation.[5,6,24] Tsekouras *et al.*[11] confirmed this correlation between impact parameter and product vibrational state in an extensive beam-gas study of this reaction. The peak locations of the specific opacity functions were found to vary monotonically from 4.1 Å for $v=4$ to 1.2 Å for $v=18$.

The information on the energy partitioning and the variation of the adjustable parameter ΔE_v as a function of E_{mp}, presented in Tables II, and IV–VII, demonstrate that the product recoil increases with collision energy. The change in the magnitude of the recoil for BaI($v=0$) is approximately 1.5 kcal/mol for a change of approximately 10 kcal/mol in collision energy. Still, owing to its light mass, the departing H atom has a velocity of a few thousand meters per second for such a recoil energy.

The product recoil also appears to increase with increasing product vibration. Therefore, as the vibrational level is increased, the shift in the peak location of the product rotational distributions appears at lower rotational quantum numbers than those predicted simply by conservation of energy. The same behavior was observed in the beam-gas experiments of Tsekouras *et al.*,[11] who suggested as possible explanations either an increase in product recoil with vibrational excitation or a strong velocity dependence in the selection of product vibrational level. Our results indicate a clear trend in the variation of the recoil energy. Because the present study contains information from only the three lowest vibrational levels, we are not in a position to extend with confidence the trend to higher vibrational levels.

The ΔE_v values we find correspond to the difference between the BaI bond dissociation energy and the product recoil energy. The dissociation energy for BaI has been found to be $D_0^o(\mathrm{BaI}) = 77.7 \pm 2$ kcal/mol.[9] Consequently, an

associated uncertainty would exist if we were to use the value of D_0^o(BaI) to extract the product recoil energy. Our results, while within the error limits of the previous determination, indicate that the estimate of 77.7 kcal/mol is rather too small. Moreover, our findings are much closer to the upper limit of 78.5±0.5 kcal/mol determined by Johnson *et al.*[49] This observation is also consistent with the results of the crossed-beam experiments by Vaccaro *et al.*[18]

As mentioned, the relative velocity plays a central role in controlling the maximum energetically allowed impact parameter. This result is, in essence, the velocity dependence of the specific opacity function confirmed in our experiments. Such a picture, however, is not complete at very low relative velocities. As the collision energy is decreased, the maximum impact parameter that conservation of energy dictates increases. Beyond a certain limiting value, impact parameters should cease being reactive. The value of the maximum reactive impact parameter at very low collision energies depends on the attractive part of the two-body potential and is determined by an angular momentum barrier, also known as a centrifugal barrier.[7] Thus, a transition must occur in the mechanism that determines $b_{\max}$; at low collision energies this mechanism is the centrifugal barrier, whereas at sufficiently high collision energies it is the law of conservation of energy. These are the two mechanisms that determine the reaction cross section. A necessary condition for the crossover to an energy-controlled $b_{\max}$ is the sufficiently large magnitude of the reactive impact parameter. Therefore, the interplay of these two mechanisms that control the cross section becomes important for a wide class of reactions that exhibit large cross sections, such as stripping or ion-molecule reactions.

In their theoretical investigation of the effects of kinematic constraints, Siegel and Schultz[6] identified these two processes and predicted their effects by performing quasiclassical trajectory calculations on various types of potential surfaces. The available experimental results for the reactions of Ba with HCl and HBr indicated that $b_{\max}$ was determined by a centrifugal barrier at all studied collision energies. In contrast, the reaction of Ba+HI provides an example of the interplay between these two mechanisms that determine the cross section.

A simple estimate of the range of relative velocities at which the transition in mechanism occurs would be of interest. In simulations of the reaction of Ba with HCl at 2.5 kcal/mol, the centrifugal barrier was found to set a limit of 5.15 Å for the maximum allowed impact parameter.[6] For Ba+HI, use of an exp-six potential[50,51] yields a value of 5 Å at 5 kcal/mol. For this estimate, elastic scattering data were used for the potential parameters that were obtained in studies of the reaction of K with HI,[52] as well as the value of 4.5 Å for the crossing of the ionic Ba^+–HI^- and the covalent Ba–HI potential curves.[19] Figure 14 shows the constraints of the angular momentum barrier and energy conservation on the $b_{\max}$ and $v_{\rm rel}$ values of the reactive encounters.

The transition from energy conservation-controlled to angular momentum-controlled $b_{\max}$ has a significant effect in the specific opacity functions for different vibrational levels,

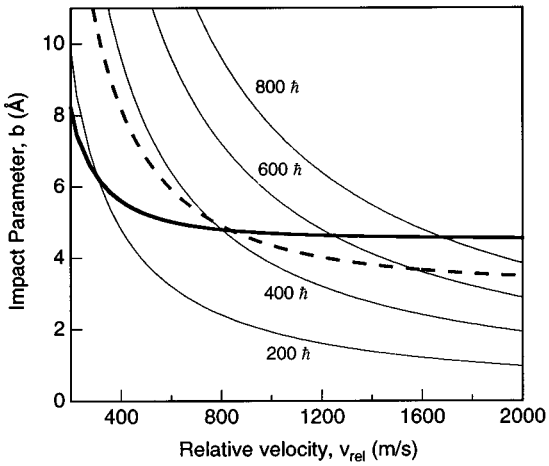

FIG. 14. The maximum allowed $b_{\max}$ for each value of $v_{\rm rel}$ as governed by the centrifugal barrier (thick solid line) and energy conservation (dashed line). The thin solid lines represent combinations that have constant angular momentum, as indicated. The space is partitioned into reactive and nonreactive combinations of b and $v_{\rm rel}$. At approximately 800 m/s, a transition occurs in the mechanism that dictates $b_{\max}$.

in particular, the lowest ones. The centrifugal barrier at low collision energies does not discriminate between different vibrational levels. In this collision energy regime, $b_{\max}$ shows a relative velocity dependence, but its value is the same regardless of product vibrational level. In contrast, the maximum impact parameter, as determined by conservation of energy, not only decreases with collision energy, but is *different* for different vibrational levels. At a relative velocity of 940 m/s, for example, the impact parameter cutoff is 4.60, 4.53, and 4.46 Å for BaI product in $v=0$, 1, and 2, respectively. In the high collision energy limit, $b_{\max}$ is largest for product in $v=0$ and becomes smaller as the vibrational excitation of the BaI is increased. Thus, a narrow range of impact parameter with a width of approximately 0.06 Å leads *exclusively* to formation of BaI($v=0$), the narrow range of b adjacent to it can produce *only* BaI($v=1$) *and* BaI($v=0$), and so forth. Consequently, a local maximum should appear at $v=0$ in the vibrational population distribution, which is the signature of a reaction cross section controlled by energy conservation.

To our knowledge, no experimental observation of such behavior has been reported before. Siegel and Schultz,[6] in their thorough three-dimensional trajectory study on the reaction of Ba with HCl using various potential energy surfaces, encountered such behavior for a hyperbolic map function surface. The trajectories indicated three features as signatures of the transition from low collision energies to the regime where $b_{\max}$ is defined by conservation of energy at large enough collision energies. First, almost all the available energy appears as product rotational energy. Such behavior is a manifestation of the kinematics and is, in essence, the reason for which the conservation of energy determines $b_{\max}$: As the relative velocity is increased, the mass combination increasingly constrains the available energy to appear as product rotation until a limit is reached, past which reac-

tion would lead to product with rotational energy greater than the total energy available. This limit is the very point at which conservation of energy controls the cross section. Second, a local maximum appears at vibrational level $v=0$ of the previously bell-shaped product vibrational distribution. The origin of this second peak was discussed in the preceding paragraph. The third indication for the change in mechanism is a breakdown of the $|\mathbf{J}_{\text{prod}}|=|\mathbf{L}_{\text{reag}}|$ propensity rule that the kinematic constraints dictate. At high collision energies, the calculations of Siegel and Schultz revealed such a deviation, in which the product rotational angular momentum in the most highly excited states gradually becomes smaller than the reagent orbital angular momentum. The larger the magnitude of the angular momentum, the more significant is this deviation. Experiments for Ba+HCl in the range of collision energies between 2.5 and 6.9 kcal/mol, however, did not reproduce the aforementioned behavior and showed product vibrational distributions independent of the collision energy.[3]

The reaction of Ba with HI appears to exhibit all three features, indicating a transition in the mechanism determining the cross section. Under the conditions of the crossed-beam experiments, the reaction product was found to have rotational excitation very close to the energetic limit. Results from studies in crossed-beam and beam-gas conditions revealed the appearance of pronounced features in the lowest vibrational levels of the product vibrational distribution in the range of 5 kcal/mol. In addition, the previously observed trend, in which the product recoil energy increases with collision energy, is an indication of a deviation from the $|\mathbf{J}_{\text{prod}}|=|\mathbf{L}_{\text{reag}}|$ propensity rule. The greater the collision energy, the larger the product recoil and orbital angular momentum and, consequently, the more significant the breakdown of the kinematic constraint. Therefore, the observed behavior for this reaction system indicates that the two previously described mechanisms are present and a transition occurs between them as a function of the collision energy.

The appearance of the second local maximum merits further discussion. Because we were able to extract information on the reactive impact parameters, we can investigate whether the specific opacity functions we have determined are consistent with the observed bimodality in the vibrational population distributions. Figure 15 presents a comparison of the effects of the two mechanisms on the specific opacity functions for BaI($v=0$), BaI($v=1$), and BaI($v=2$). As a starting point, we used the deduced specific opacity functions for the three lowest vibrational levels $v=0$, 1, and 2. The width parameter was chosen to be 0.7 Å, a value representative of the determined width parameters from our simulations. The peak locations for $v=0$, 1, and 2 also correspond to the values determined in the preceding analysis. For the comparison we can assume that the relative heights of the specific opacity functions are the same for these neighboring levels. Such an assumption does not affect the validity of the comparison. The left panels represent the energy regime just below the transition, whereas the situation in the high collision energy regime is presented in the right panels. Figures 15(a) and 15(d) show specific opacity functions without taking into account any energy or angular momentum constraints. Figure 15(b) displays the truncation of the specific opacity functions at 5 Å for $v=0$, 1, and 2 by the presence of a centrifugal barrier. In contrast, Fig. 15(e) shows the truncation of the specific opacity functions as controlled by conservation of energy at a collision energy of 6.1 kcal/mol, i.e., right after the transition is expected to have occurred. In Figs. 15(c) and 15(f), the corresponding normalized specific opacity functions are shown. For each value of the impact parameter b, the values of the specific opacity function for $v=0$, 1, and 2 are each divided by their sum. The normalization is motivated by the fact that the total reaction probability has been calculated for similar kinematically constrained systems to have the form of a step function with a unit probability at each reactive impact parameter.[6] In all panels of Fig. 15, the units of the abscissa have been kept the same to display explicitly the effect of the normalization.

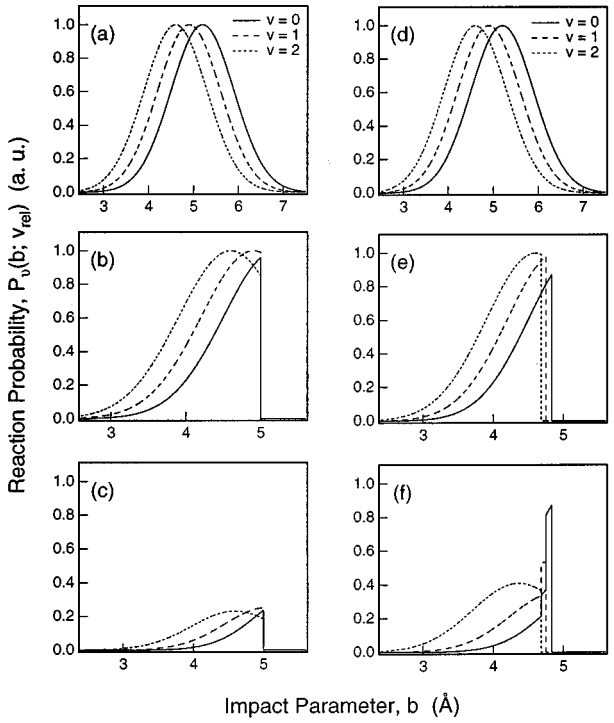

FIG. 15. Specific opacity functions for vibrational levels $v=0$, 1, and 2 are shown as well as the truncation at $b_{\max}$ owing to an angular momentum barrier and conservation of energy, at low and high collision energies, respectively. See text for detailed explanation.

The difference in the appearance of the specific opacity functions between the two energy regimes is remarkable. Figure 15(c) displays the normalized specific opacity functions for $v=0$, 1, and 2 as truncated by the centrifugal barrier. They are rather broad and, as expected, the reaction probability is shared between the overlapping specific opacity functions. The relative order of the integrated reaction probabilities of Fig. 15(c) is $v=0<v=1<v=2$, in agreement with the trend observed in Figs. 3(a) and 5(a). Because vibrational levels higher than $v=2$ were not included in the comparison, the tails of the specific opacity functions at

small impact parameters are overestimated to some extent. For the higher collision energies, where the maximum impact parameter is dictated by conservation of energy, the truncation of the specific opacity functions depends on the product vibrational level and results in sharp peaks, as shown in Fig. 15(f). These sharp reaction probability peaks have a width of approximately 0.06 Å. For this reason, the specific opacity functions in the crossed-beam experiments are narrow and sharply peaked. In fact, as first noted by Vaccaro *et al.*,[18] a Dirac delta function as specific opacity function for BaI($v=0$) can yield simulated rotational distributions that reproduce the main features of the experimentally observed ones. This observation was further investigated and found to hold for the collision energy range and the vibrational levels studied in our experiments. Finally, we note that the relative probability for the sharp peaks of the specific opacity functions at high collision energy is much larger than the maximum of the reaction probability for the same vibrational level at low collision energy. This effect is the source of the additional peak that appears in the lowest levels of the product vibrational distribution at high collision energies. Again, because vibrational states higher than $v=2$ are not included, the specific opacity functions shown are overestimated for low impact parameters. Moreover, had a specific opacity function been included for BaI($v=3$), a sharp peak would have appeared in the specific opacity function for BaI($v=2$). We note that the normalization of the truncated Gaussians with respect to each other does not contradict the simulations of the experimental results (where unnormalized functions were used), because this treatment does not alter their overall features; even in the high collision energy regime, where the change in the shape of the specific opacity functions between Figs. 15(e) and 15(f) appears to be dramatic, the specific opacity functions remain narrow, sharply peaked functions.

Furthermore, we could expect that at very large collision energies the truncation of the specific opacity functions of the lowest vibrational levels is so extensive that only a small fraction of the tail of the gaussian function is reactive. Then, the effect of the appearance of a second maximum in the vibrational population distribution as collision energies rise from low to high should not be so pronounced. Such an observation is consistent with the previous crossed-beam results of Vaccaro *et al.*[18,53] at 7.6 kcal/mol and at approximately 12 kcal/mol, as shown in Fig. 16. When compared with the intensity of the higher vibrational levels, the intensity of the three lowest vibrational levels at 12 kcal/mol is substantially lower than that at 7.6 kcal/mol. Therefore, we can conclude that the overall behavior appears consistent with a transition between the two mechanisms that control the cross section.

In light of this information, we reexamine the specific opacity function for BaI($v=0$) under beam-gas conditions. The product rotational distribution for BaI($v=0$) appears bimodal and has a peak around $J=420.5$.[1] Tsekouras *et al.*[11] were not able to determine a specific opacity function for BaI($v=0$) produced under beam-gas conditions and noted that application of conservation of energy indicates that the peak of the distribution be produced by the ''fast'' tail of the

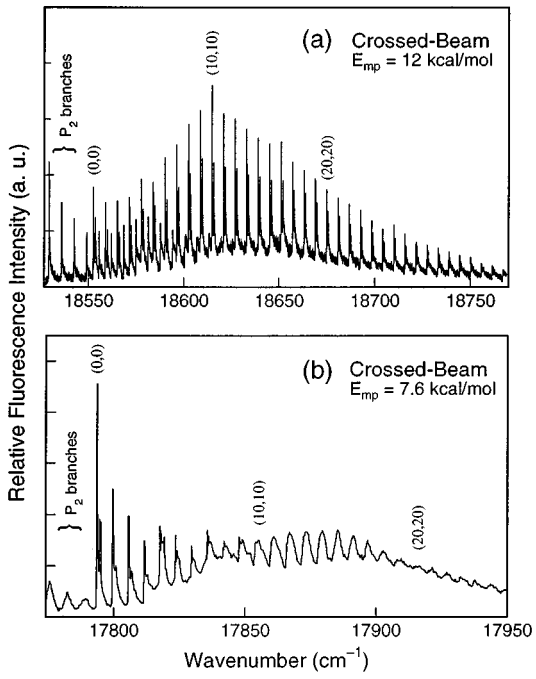

FIG. 16. Smoothed spectra covering the BaI $C\ ^2\Pi_{1/2}-X\ ^2\Sigma^+$ BaI $C\ ^2\Pi_{3/2}-X\ ^2\Sigma^+$ $\Delta v=0$ sequences. The spectra are recorded under crossed-beam conditions at 7.6 kcal/mol and approximately 12 kcal/mol. Panel (a) is taken from Ref. 20 and panel (b) is taken from Ref. 18.

relative velocity distribution. Consideration of the picture provided by the interplay between the two mechanisms that determine the cross section seems to provide the interpretation to the observed behavior. When these two mechanisms, whose effect on the specific opacity function was displayed in Fig. 15, are combined, the product BaI($v=0$) rotational distribution under beam-gas conditions can be successfully simulated in a qualitative manner. Such a simulation is presented in Fig. 17.

The specific opacity function model employed for the simulation of Fig. 17 consists of two functions: a Gaussian function that is truncated as that in Fig. 15(c) for relative velocities below 800 m/s, and a second one that is truncated by conservation of energy for relative velocities above 800 m/s. The former function models the specific opacity function at relative velocities in which it is controlled by a centrifugal barrier, whereas in the latter, conservation of energy plays the controlling role. In other words, the specific opacity function that corresponds to the tail in the fast side of the relative velocity distribution gives rise to the product rotational states of BaI near the energetic limit. The values of the deduced parameters for the two functions used in the fit are presented in the caption of Fig. 17.

The large reaction probability for the sharply peaked specific opacity functions in the high collision energy regime is responsible for the location of the rotational distribution maximum. The intensities of this maximum and of the second peak at approximately $J=365.5$, which corresponds to the maximum of the relative velocity distribution, are simi-

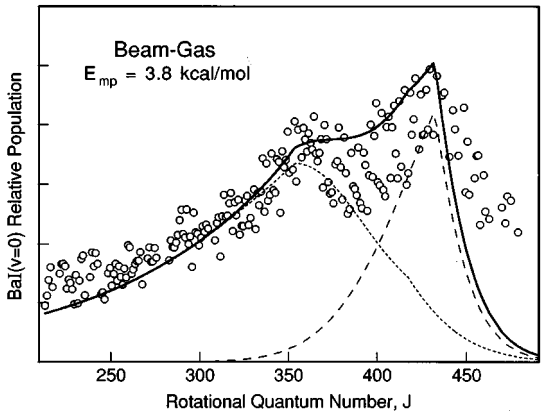

FIG. 17. Simulation of the beam-gas data of Fig. 7(a). For relative velocities below 800 m/s, the specific opacity function is modeled by a Gaussian function that (1) is truncated at $b>5$ Å and (2) has the parameters $b_0=5.2$ Å, $\sigma_0=0.4$ Å, and $\Delta E_0=79.0$ kcal/mol. The resulting product distribution is represented by the dotted line. For relative velocities above 800 m/s, the specific opacity function is modeled by a Gaussian function that (1) is truncated at the energetic limit and (2) has the parameters $b_0=5.2$ Å, $\sigma_0=0.5$ Å, and $\Delta E_0=79.6$ kcal/mol (dashed line). The sum of the two contributions is represented by the solid line. The two functions were independently scaled to best fit the experimental distribution.

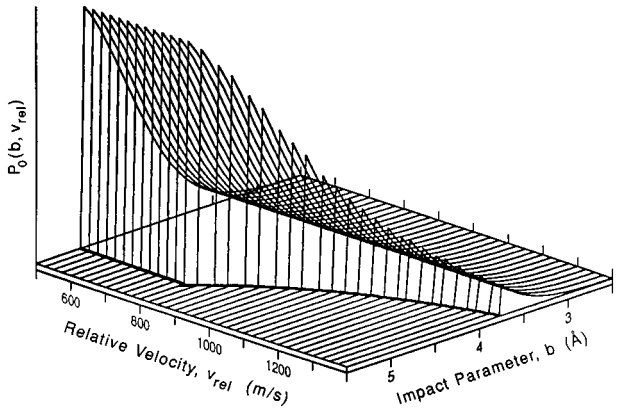

FIG. 18. The deduced specific opacity function surface for BaI($v=0$). The plotted function has the parameters $b_0=5.2$ Å, $\sigma_0=0.5$ Å, and $\Delta E_0=79.4-0.14\ E_{\rm col}$, where $E_{\rm col}$ is the center-of-mass collision energy. For relative velocities between 500 and 800 m/s, the centrifugal barrier does not allow the reaction to occur for impact parameters greater than approximately 5 Å. Above 800 m/s, the specific opacity function is truncated by conservation of energy. As the relative velocity increases, the maximum allowed value of the impact parameter becomes smaller.

lar; the ''fast'' tail represents only a fraction of the relative velocity distribution, but this fact is counterbalanced by the sharply peaked specific opacity function, once it is controlled by conservation of energy. Having shown the changes that occur in the shape of the specific opacity functions as the collision energy is changed, we note that the use in the simulation of a truncated Gaussian function for both mechanisms is rather simplistic. Nevertheless, the simulation succeeds in confirming the expected behavior from the transition in the mechanism that controls the form of the specific opacity functions.

We combine the acquired information on the behavior of the specific opacity function and present a detailed picture that includes its relative velocity dependence over a wide range of collision energies. Such an example is presented in Fig. 18, in which the ''specific opacity surface'' for BaI($v=0$) is shown. In this figure, the reaction probability for BaI product in vibrational level $v=0$ is plotted as a function of impact parameter and reagent relative velocity. Similar behavior is found for the specific opacity functions of product BaI in $v=1$ and $v=2$. For higher vibrational levels, the effect of energy conservation, as well as the importance of the angular momentum barrier, become gradually less important because these specific opacity functions are mapped into smaller and smaller impact parameters. In fact, an interesting situation arises for the very large vibrational levels. Under crossed-beam conditions, vibrational levels up to $v=34$ have been reported.[9] Owing to the weighting factor $2\pi b$, all the very high vibrational levels are expected to have weighted specific opacity functions that peak at similar impact parameters. This prediction is supported by beam-gas results for $v=18-28$, for which the peak of the rotational distribution was found near 100 $\hbar$, regardless of the vibrational excitation.[11,54] Thus, significant rotational excitation exists, even in the highest product vibrational states. Such behavior can also explain why we find that the BaI bond dissociation energy is larger than the previous determination of 77.7 ± 2 kcal/mol, for which the highest vibrational levels were assumed rotationless.[9]

Why has a bimodality similar to that of the Ba+HI reaction not been observed for Ba+HCl and Ba+HBr? The answer might be that the Ba+HCl and Ba+HBr studies were not carried out at large enough collision energies. Neither the exoergicity nor the kinematic constraints are the same for these reactions. Moreover, the location of the centrifugal barrier depends on the long-range attractive part of the interaction potential and can vary between the different reaction systems. The quasiclassical trajectory study of Siegel and Schultz[6] indicated that the mechanism that controls the maximum allowed impact parameter is sensitive to the features of the potential energy surface.

Is the Ba+HI reaction sensitive to the form of the potential energy surface? Our data cannot be inverted simply to find the form of the potential, but the results we have obtained contain more information than solely what is predicted from this special mass combination. Our study shows that the observed behavior for the exothermic reaction of Ba with HI is consistent with a direct abstraction mechanism that involves an electron jump at the curve crossing between the covalent Ba–HI potential and the ionic Ba^+–HI^- potential. The possibility that some trajectories sample the deep H–Ba–I insertion well cannot be excluded, although we have no evidence for their existence. The attractive character of the surface is attributed to the sudden change in bonding nature from covalent to ionic and is manifest by substantial product vibrational excitation. In addition, the long-range attractive part of the potential appears to be shallow and bar-

rierless. The long-range attractive potential, the location of the avoided crossing for the Ba–HI and Ba^+–HI^- curves (estimated to occur at 4.5 Å), and the kinematic constraints of the mass combination cause the crossover in the mechanism that controls the maximum allowed impact parameter. Our experimental observations show the reaction of Ba with HI to exhibit primarily the direct behavior that Cruse, Dagdigian, and Zare[4] observed for the reactions of barium atoms with hydrogen halide molecules. In addition, we observe a transition between the two mechanisms that determine the reaction cross section when the collision energy is varied below and above 5 kcal/mol: At low relative velocities, the maximum reactive impact parameter is defined by an angular momentum barrier, whereas at high relative velocities, it is determined by conservation of energy.

VII. SUMMARY AND CONCLUSIONS

Recent and previous experiments in crossed-beam and beam-gas configurations indicate a bimodality in the BaI product vibrational and rotational distributions. For collision energies smaller than 5 kcal/mol, the product vibrational distribution is bell shaped and peaks at $v=12$. For collision energies larger than 5 kcal/mol, a second maximum appears in the vibrational distribution at $v=0$. The rotational distributions also reveal a telltale sign of bimodality and have maxima at unexpectedly large rotational quantum numbers.

For the crossed-beam experiments, we exploited the capabilities of a scheme for the selective detection of the LIF from the reaction product BaI. Consequently, well-characterized experiments produced high-resolution results for BaI($v=0,1,2$) in a broad range of collision energies. The recorded spectra were converted into product rotational distributions. These results showed a trend in which the peak of the rotational distribution shifts to higher rotational quantum number with collision energy. In addition, the peaks for the product rotational distributions for BaI($v=1$) and BaI($v=2$) appear at lower rotational excitation as the vibrational energy is increased. Finally, the product recoil energy appears to increase with collision energy in a similar manner for all vibrational levels we studied.

The kinematically constrained nature of this reaction system allows the extraction of information on its impact parameter dependence. A Gaussian function of reactive impact parameters that (1) is truncated at the energetic limit at high collision energies, (2) is subject to a centrifugal barrier at low collision energies, and (3) accounts for the increase of the product recoil energy as the collision energy is increased, successfully models the specific opacity functions of the three lowest vibrational levels. This model simulates the observed product rotational distributions for the broad range of collision energies of our experiments. The specific opacity functions we have deduced are sharply peaked and confirm the aforementioned trend in product recoil energy. Consequently, the result is a direct mapping of reactive impact parameters to product rotational states for each product vibrational level. Our results are also consistent with the well-established correlation that associates smaller impact parameters with larger vibrational excitation.

Analysis of the specific opacity functions reveals that two mechanisms operate to control the maximum allowed reactive impact parameter: a centrifugal barrier at low collision energies and conservation of energy at high collision energies. A transition is observed between the two mechanisms that occurs at a collision energy of approximately 5 kcal/mol. This transition results in a dramatic change in the shape of both the product vibrational and rotational distributions. The effect is expected to be more pronounced for the lowest vibrational levels. Understanding of the competition between these two mechanisms that determine the cross section provides an interpretation for the behavior of the Ba+HI reaction derived from the present study that is consistent with the results of extensive studies over the past 25 years. In addition, this interpretation clarifies the origin of the observed bimodality. Moreover, such a crossover is expected to be general for reactions that have large cross sections.

In conclusion, we note that the modeling of the BaI specific opacity functions over a broad collision energy range has provided an extremely detailed picture for this kinematically constrained reaction system and has proven to be a powerful tool for elucidating microscopic details of the relation between reagent approach geometry and reaction outcome, as well as for revealing the mechanisms by which the magnitudes of reactive cross sections are determined.

ACKNOWLEDGMENTS

K.S.K. wishes to thank A. A. Tsekouras and J. Cai for their help in some of the presented experiments and B. Girard, S. Falcinelli, and F. Fernández-Alonso for helpful comments and discussions. Financial support from the U.S. National Science Foundation under Grant No. CHE-93-22690 is gratefully acknowledged.

[1] R. N. Zare and K. S. Kalogerakis, *The R. A. Welch Foundation 38th Conference on Chemical Research* (Houston, TX, 1994), p. 45.
[2] R. L. Jaffe, M. D. Pattengill, F. G. Mascarello, and R. N. Zare, J. Chem. Phys. **86**, 6150 (1987).
[3] A. Siegel and A. Schultz, J. Chem. Phys. **72**, 6227 (1980).
[4] H. W. Cruse, P. J. Dagdigian, and R. N. Zare, Faraday Discuss. Chem. Soc. **55**, 277 (1973).
[5] D. R. Herschbach, Faraday Discuss. Chem. Soc. **33**, 149 (1962).
[6] A. Siegel and A. Schultz, J. Chem. Phys. **76**, 4513 (1982).
[7] R. D. Levine and R. B. Bernstein, *Molecular Reaction Dynamics and Chemical Reactivity* (Oxford U.P., Oxford, 1987).
[8] B. Soep, C. J. Whitham, A. Keller, and J. P. Visticot, Faraday Discuss. Chem. Soc. **91**, 191 (1991).
[9] P. H. Vaccaro, D. Zhao, A. A. Tsekouras, C. A. Leach, W. E. Ernst, and R. N. Zare, J. Chem. Phys. **93**, 8544 (1990).
[10] C. Linton, J. Mol. Spectrosc. **69**, 351 (1978).
[11] A. A. Tsekouras, C. A. Leach, K. S. Kalogerakis, and R. N. Zare, J. Chem. Phys. **97**, 7220 (1992).
[12] C. Noda, J. S. McKillop, M. A. Johnson, J. R. Waldeck, and R. N. Zare, J. Chem. Phys. **85**, 856 (1986).
[13] D. Zhao, P. H. Vaccaro, A. A. Tsekouras, C. A. Leach, and R. N. Zare, J. Mol. Spectrosc. **148**, 226 (1991).
[14] C. A. Leach, A. A. Tsekouras, and R. N. Zare, J. Mol. Spectrosc. **153**, 59 (1992).
[15] C. A. Leach, J. R. Waldeck, C. Noda, J. S. McKillop, and R. N. Zare, J. Mol. Spectrosc. **146**, 465 (1991).

[16] M. A. Johnson, C. Noda, J. S. McKillop, and R. N. Zare, Can. J. Phys. **62**, 1467 (1984).
[17] M. A. Johnson, C. R. Webster, and R. N. Zare, J. Chem. Phys. **75**, 5575 (1981).
[18] P. H. Vaccaro, A. A. Tsekouras, D. Zhao, C. A. Leach, and R. N. Zare, J. Chem. Phys. **96**, 2786 (1992).
[19] D. Zhao, Ph.D. thesis, Stanford University, 1991.
[20] A. A. Tsekouras, Ph.D. thesis, Stanford University, 1992.
[21] C. Noda, Ph.D. thesis, Stanford University, 1987.
[22] J. S. McKillop, Ph.D. thesis, Stanford University, 1987.
[23] M. A. Johnson, Ph.D. thesis, Stanford University, 1983.
[24] C. Noda and R. N. Zare, J. Chem. Phys. **86**, 3968 (1987).
[25] W. S. Hartree, J. P. Simons, and A. Gonzalez-Ureña, J. Chem. Soc. Faraday Trans. **86**, 17 (1990).
[26] R. Altkorn, F. E. Bartoszek, J. Dehaven, G. Hancock, D. S. Perry, and R. N. Zare, Chem. Phys. Lett. **98**, 212 (1983).
[27] Z. Karny, R. C. Estler, and R. N. Zare, J. Chem. Phys. **69**, 5199 (1978).
[28] R. Zhang, D. J. Rakestraw, K. G. McKendrick, and R. N. Zare, J. Chem. Phys. **89**, 6283 (1988).
[29] H. Schor, S. Chapman, S. Green, and R. N. Zare, J. Phys. Chem. **83**, 920 (1979).
[30] H. Schor, S. Chapman, S. Green, and R. N. Zare, J. Chem. Phys. **69**, 3790 (1978).
[31] J. M. Alvariño and A. Laganà, Chem. Phys. Lett. **144**, 558 (1988).
[32] J. M. Alvariño and A. Laganà, Chem. Phys. Lett. **168**, 448 (1990).
[33] J. M. Alvariño, M. L. Hernández, J. Margarido, and A. Laganà, J. Chem. Phys. **93**, 1082 (1990).
[34] S. Chapman, J. Chem. Phys. **81**, 262 (1984).
[35] X. Liu and J. N. Murrell, J. Chem. Soc. Faraday Trans. **87**, 435 (1991).
[36] X. Liu, J. Chem. Soc. Faraday Trans. **90**, 249 (1994).
[37] A. Laganà, M. Paniagua, and J. M. Alvariño, Chem. Phys. Lett. **168**, 441 (1990).
[38] A. Laganà, M. Dini, and E. Garcia, J. Phys. Chem. **95**, 8379 (1991).
[39] J. M. Alvariño and A. Laganà, J. Chem. Phys. **95**, 998 (1991).
[40] J. M. Alvariño and A. Laganà, J. Phys. Chem. **96**, 3587 (1992).
[41] J. M. Alvariño, L. Cuadrado, and A. Laganà, J. Chem. Phys. **98**, 5102 (1993).
[42] J. M. Alvariño, L. Cuadrado, M. L. Hernández, and A. Laganà, Chem. Phys. Lett. **241**, 408 (1995).
[43] C. K. Man and R. C. Estler, J. Chem. Phys. **75**, 2779 (1981).
[44] H. J. Loesch and F. Stienkemeier, J. Chem. Phys. **100**, 741 (1994).
[45] Z. Karny and R. N. Zare, J. Chem. Phys. **68**, 3360 (1978).
[46] A. Gupta, D. S. Perry, and R. N. Zare, J. Chem. Phys. **72**, 6250 (1980).
[47] D. Zhao and R. N. Zare, J. Chem. Phys. **97**, 6208 (1992).
[48] M. Albertí, X. Giménez, A. Aguilar, and A. G. Ureña, Mol. Phys. **85**, 949 (1995).
[49] M. A. Johnson, J. Allison, and R. N. Zare, J. Chem. Phys. **85**, 5723 (1986).
[50] E. A. Mason, J. Chem. Phys. **22**, 169 (1954).
[51] E. A. Mason, J. Chem. Phys. **26**, 667 (1957).
[52] M. Ackerman, E. F. Greene, A. L. Moursund, and J. Ross, J. Chem. Phys. **25**, 389 (1964).
[53] P. H. Vaccaro, A. A. Tsekouras, D. Zhao, C. A. Leach, and R. N. Zare (unpublished).
[54] A. A. Tsekouras, K. S. Kalogerakis, and R. N. Zare (unpublished).